



Cite this: *Dalton Trans.*, 2021, **50**, 6784

Received 21st March 2021
Accepted 5th May 2021

DOI: 10.1039/d1dt00927c

rsc.li/dalton

Effect of different oxide and hybrid precursors on MOF-CVD of ZIF-8 films†

Alexander John Cruz,^a Giel Arnauts,^{a,b,c} Martin Obst,^a Dmitry E. Kravchenko,^a Philippe M. Vereecken,^{a,c} Steven De Feyter,^d Ivo Stassen,^a Tom Hauffman^b and Rob Ameloot^{*a}

Chemical vapor deposition of metal–organic frameworks (MOF-CVD) will facilitate the integration of porous and crystalline coatings in electronic devices. In the two-step MOF-CVD process, a precursor layer is first deposited and subsequently converted to a MOF through exposure to linker vapor. We herein report the impact of different metal oxide and metalcone layers as precursors for zeolitic imidazolate framework ZIF-8 films.

To leverage the properties of metal–organic frameworks (MOFs) in electronic devices, robust thin film deposition processes are required.^{1,2} Chemical vapor deposition of MOFs (MOF-CVD)³ has been demonstrated on wafer-scale in a clean-room setting,⁴ and has shown potential in sensing,^{5,6} energy storage,^{7,8} membrane separations,^{9,10} and nanoelectronics.¹¹ The two-step MOF-CVD process was initially demonstrated by depositing a metal oxide (*e.g.*, ZnO or CoO_x) followed by exposure to the linker vapor (2-methylimidazole; HmIM) to grow ZIF-8 or ZIF-67 films under mild conditions (<150 °C).^{3,4,11} The oxide-to-MOF conversion was found to progress in three stages: (1) linker adsorption, (2) reaction, and (3) crystallization of the framework. Due to the porosity of ZIF-8, a pronounced thickness increase occurs when the MOF is formed from the dense oxide precursor: theoretically 16× for an ideal ZnO crystal, experimentally 10× for a defective ZnO precursor.^{3,4} This behavior results in a sigmoidal increase in the layer thickness during MOF-CVD.^{3,4,12} Since its first dem-

onstration, MOF-CVD has been extended to other MOF materials.^{4,9–16} Previously, we studied the effects of precursor layer thickness, water vapor, and linker exposure time on the precursor conversion rate and the morphology of the resulting MOF layers.⁴ The accelerating effect of moisture is partly due to surface hydroxylation and hydration, which facilitates the oxide-to-MOF transformation.^{3,4} Nevertheless, little is known about the effect of the precursor type (*e.g.*, defect density in oxide layers, oxide *versus* hybrid precursors) on the conversion rate, morphology, and porosity of the resulting MOF layers.

Here, we investigate the effect of different precursor layers deposited by methods common in microfabrication (Fig. S1†): (1) ZnO and (2) aluminum-doped ZnO (AZO) by atomic layer deposition (ALD), (3) ZnO by sputtering (physical vapor deposition, PVD), and (4) hybrid zinc-based metalcones ('zinc-cones'), grown from diethylzinc and either ethylene glycol or glycerol by molecular layer deposition (MLD). In addition, the effects of precursor annealing at 850 °C and water vapor exposure are investigated. The precursor-to-MOF conversion process was performed in a MOF-CVD reactor under previously optimized conditions.⁴

When exposed to HmIM vapor, all oxide precursors converted at least partially to ZIF-8, irrespective of annealing or added water vapor, as shown by grazing-incidence X-ray diffraction (GI-XRD, Fig. S2 and S3†). Nevertheless, the *in situ* ellipsometry data shows that the oxide-to-MOF conversion kinetics depend on the precursor type (Fig. 1a). For the oxides, a thickness of approximately 3 nm was consistently used to compare the characteristic growth profiles during precursor-to-MOF transformation. X-ray photoelectron spectroscopy (XPS O 1s, Fig. S4, S5 and Table S1†) was used to probe the defect density in the oxide precursor layers and shows varying contributions from Zn-bound O²⁻, OH⁻, and surface-adsorbed water.^{17,18} The 'hydroxylation degree' was calculated from the O 1s spectrum as the ratio of the summed Zn–OH and Zn–H₂O area contributions to that of Zn–O. This value is higher for oxide films with a lower density (measured by XRR), likely due to the presence of hydroxyl defects throughout the film (Fig. 1b).^{4,17,18} The hydroxylation degree increases by exposing the oxides to

^aCentre for Membrane Separations, Adsorption, Catalysis, and Spectroscopy for Sustainable Solutions (cMACS), Department of Microbial and Molecular Systems, KU Leuven – University of Leuven, Celestijnenlaan 200F, Leuven, 3001, Belgium. E-mail: rob.ameloot@kuleuven.be

^bResearch Group of Electrochemical and Surface Engineering (SURF), Department of Materials and Chemistry (MACH), Vrije Universiteit Brussel, Pleinlaan 2, Brussels, 1050, Belgium

^cimec, Kapeldreef 75, Leuven, 3001, Belgium

^dDivision of Molecular Imaging and Photonics, Department of Chemistry, KU Leuven – University of Leuven, Celestijnenlaan 200F, Leuven, 3001, Belgium

†Electronic supplementary information (ESI) available: Methods, in-depth characterization of the samples using various techniques (XPS, XRR, AFM, *in situ* and *ex situ* ellipsometry, Kr sorption, and XRD). See DOI: 10.1039/d1dt00927c

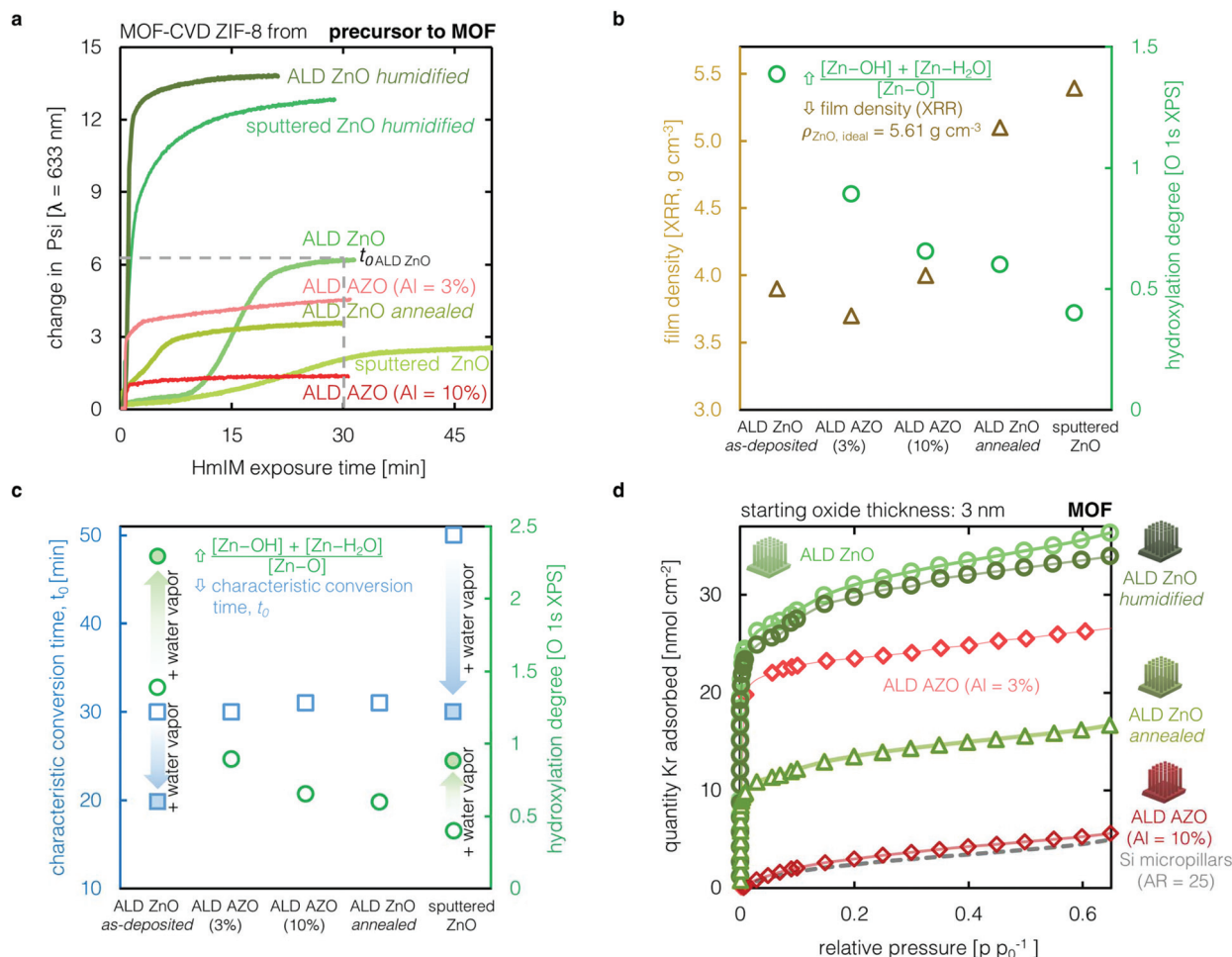


Fig. 1 MOF-CVD ZIF-8 from different ZnO precursors. (a) *In situ* ellipsometry profile of the oxide-to-MOF conversion. Correlation of the 'hydroxylation degree' determined from the XPS O 1s spectra with the (b) film density obtained via XRR, and (c) the 'characteristic conversion time', t_0 . This parameter (t_0) is defined as the time to reach a plateau in the conversion curve obtained by *in situ* ellipsometry. The t_0 for ALD ZnO is indicated in (a) for illustration. The effect of water vapor is demonstrated for ALD ZnO and sputtered ZnO (blue and green arrows). (d) Kr physisorption isotherms on high-aspect-ratio Si micropillar chips coated with different ALD oxides, before and after conversion to ZIF-8.

humidity in the MOF-CVD reactor (RH \sim 12% at 80 °C, Fig. 1c). Because a higher hydroxylation degree indicates a more defective and reactive oxide, the corresponding precursor layers are more easily converted into MOF films. This behavior is clear from the *in situ* ellipsometry data during conversion, with a faster initiation and an earlier plateau in the growth curve (Fig. 1a and c). The time at which this plateau is reached is referred to as the 'characteristic conversion time', t_0 (Fig. 1c). The oxide-to-MOF transformation involves a simultaneous change in refractive index and thickness. Modeling of the data is avoided by directly monitoring the ellipsometric angle, Psi (ψ), which is the amplitude ratio of the *p*- and *s*-polarized light reflecting from the sample.^{11,19}

When a MOF layer forms, it slows down the mass transport of linker molecules from the vapor atmosphere to any remaining oxide precursor underneath the MOF. Therefore, more defective and reactive precursor layers can result in thicker MOF films, as the reaction front can penetrate deeper before

the onset of MOF crystallization.^{3,4} When full precursor conversion is not achieved at shorter conversion times (<30 min), a second sigmoidal step may appear after extended HmIM exposures (Fig. S6†).⁴ This second conversion step may only occur for precursors with a sufficiently high hydroxylation degree and a reactor configuration that enables a high HmIM concentration. Here, our focus is on the initial MOF layer, formed at conversion times <50 min. The HmIM vapor concentration in the employed MOF-CVD reactor is diluted because of the carrier gas flow. While this reactor design enables the homogeneous and large-area coatings necessary for device fabrication, higher vapor concentrations are required if a full conversion of less reactive precursors is desired. Such conditions have been previously demonstrated, for instance in glass reactors (*e.g.*, Schlenk tubes) with a smaller volume.^{3,11}

For ALD ZnO deposited at low temperature (80 °C), the hydroxylation degree is sufficiently high to enable a rapid full conversion to ZIF-8.⁴ However, when the same layer is

annealed, or when a less defective oxide is deposited *via* sputtering, even the 3 nm precursor layer is not fully converted under the applied conditions (Fig. 1a and d). In the case of AZO, the particle morphology (Fig. S4†) is similar as in MOF-CVD ZIF-8 films grown from 3 nm ALD ZnO,⁴ and sputtered²⁰ and electroblown AZO.²¹

The porosities of MOF layers deposited on high-aspect-ratio microstructured substrates were evaluated by Kr physisorption (Fig. 1d).^{3,4,13,22} Only MOF layers resulting from ALD precursors were evaluated since a conformal coating is required, which could not be obtained *via* sputtering. Not surprisingly, the absolute Kr uptake (nmol per projected surface area) is lower for AZO and annealed ALD ZnO films, as less ZIF-8 is formed at t_0 due to the lower hydroxylation degree, passivating AlO_x content, or higher density of these precursors. These relationships are corroborated by Rutherford backscattering (RBS) and X-ray reflectivity (XRR) measurements (Fig. S7†).

Adding water vapor accelerates the ZnO-to-ZIF-8 conversion, as previously observed.^{3,4,12} Since the onset of MOF crystallization slows down the mass transfer of linker vapor to the underlying oxide, the initial conversion rate and the degree of conversion at t_0 are linked. Therefore, injecting water vapor into the reactor chamber leads to higher conversion for less reactive oxides. For instance, for sputtered ZnO, the conversion more than doubles under humidified conditions, as suggested by ellipsometry measurements. For a precursor thickness of 3 nm, the modeled PVD ZnO layer thicknesses remaining after conversion are 2 nm and 0.5 nm for MOF-CVD under dry and humidified conditions, respectively. The conversion of PVD ZnO under humidified conditions leads to increased methanol uptake, as monitored by ellipsometric porosimetry (Fig. S8†). For the annealed ALD ZnO, the AFM images reveal that the surface coverage is enhanced, from partial to full coverage, when converted under humidified conditions (Fig. S9†). In addition to accelerating the oxide-to-MOF conversion, water

vapor also facilitates crystallite ripening.⁴ Ripening also results in larger crystal facets and rougher layers (Fig. S4†). For example, for ALD ZnO, a 79% roughness increase in the resulting MOF layer is observed when converting under humidified conditions for a fixed HmIM exposure time. If not desired, these effects can be minimized by not exposing the film to humid HmIM vapor longer than needed to achieve the anticipated extent of conversion.⁴

To expand to other precursor chemistries, we explored the use of zinc glycolate (Zn-EG) and zinc glycerolate (Zn-Gly) precursors deposited *via* molecular layer deposition (MLD), Fig. S10–S12 and Table S2†. As in ALD, films deposited *via* MLD are conformal.^{3,4,23–25} These metalcone films only converted to crystalline and porous MOFs under humidified conditions, as indicated by GI-XRD and Kr physisorption (Fig. 2a and b). The resulting ZIF-8 layers were rougher and less homogenous compared to the films obtained from ALD ZnO (Fig. 2c). Together with the thickness obtained from ellipsometry, RBS measurements of the Zn-EG and Zn-Gly films show a Zn density of $9.3 \pm 0.07 \times 10^{21}$ and $7.1 \pm 0.06 \times 10^{21}$ atoms per cm^3 , respectively. These values are 67% and 74% lower than for ALD ZnO,^{3,4} and in agreement with the 3–4× thickness expansion expected when taking into account the volume per mole of Zn in Zn-EG, Zn-Gly, and ZIF-8. In contrast to the water formed during the conversion of oxide precursors, the ethylene glycol or glycerol released in the reaction of zincones with HmIM would not result in linker protonation and is unable to catalyze the Zn-EG- or Zn-Gly- to ZIF-8 transformation.^{26,27} Therefore, the addition of water vapor is needed to enable MLD zincone-to-MOF conversion. Moreover, the low volatility of these byproducts interferes with the formation of continuous films, as the ethylene glycol and glycerol droplets forming on the surface lead to micron-sized pinhole defects in the MOF film (Fig. S13†). The conversion of MLD zincones to ZIF-8 is an interplay of $\text{Zn-H}_2\text{O}/\text{Zn-OH}$ concen-

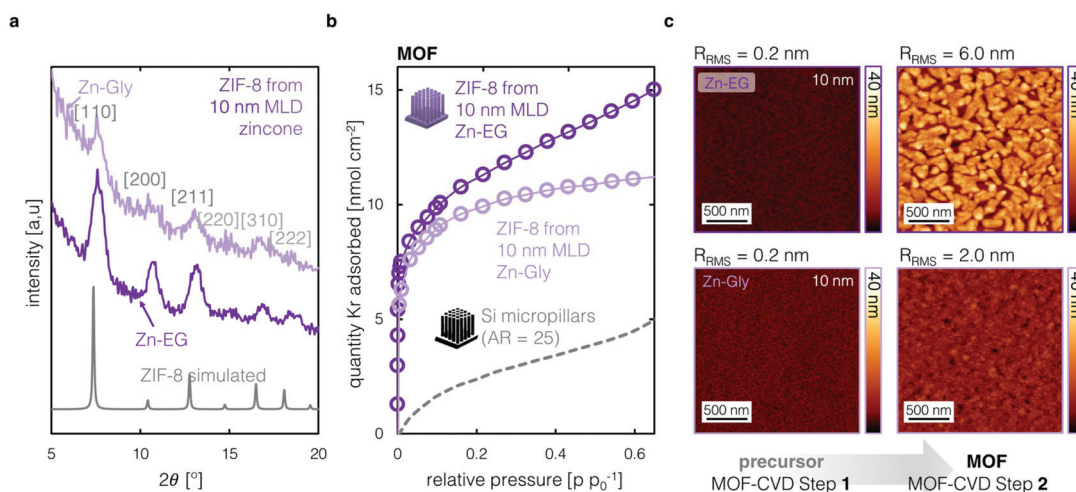


Fig. 2 ZIF-8 from MLD zincones under humidified conditions. (a) GI-XRD of the ZIF-8 films from MLD zincones (CCDC for ZIF-8: VELVOY). (b) Kr physisorption isotherms of ZIF-8 from MLD zincone precursors. (c) AFM images of the MLD zincones and the corresponding ZIF-8 layers after conversion. The R_{RMS} values are calculated for a 2×2 and $6 \times 6 \mu\text{m}^2$ probe area.

tration, precursor density, and volatility and reactivity of byproducts.^{4,28} Nevertheless, zincones can be transformed into mesoporous ZnO layers through calcination.²⁹ Up to twice as large ZIF-8 crystals are generated compared to the ones obtained from non-calcined equivalents due to the enhanced ZnO accessibility for HmIM vapor in these structured precursors (Fig. S14 and 15,† MLD Zn-Gly calcined in air, 200 °C, 2 h).⁸

In summary, the different nature of ZnO, AZO, and hybrid precursors as well as the presence of water vapor influence the kinetics of the precursor-to-MOF transformation and the resulting ZIF-8 morphology. Together with the previously reported integrated cleanroom MOF-CVD process⁴ and vapor-phase linker exchange,²⁶ these insights facilitate the fabrication of high-quality ZIF films reproducibly and reliably.

Conflicts of interest

There are no conflicts to declare.

Acknowledgements

This project has received funding from the European Research Council (ERC) under the European Union's Horizon 2020 research and innovation program, grant agreements no. 716472 (VAPORE), 765378 (HYCOAT), and 801464 (Future and Emerging Technologies-FETOPEN-1-2016-2017). The Research Foundation Flanders (FWO) is acknowledged for funding in the research projects G083016N, G85720N, 1529618N, and 1501618N, as well as the infrastructure project G0H0716N. G. A. and I. S. thank FWO for the fellowships 1SA7320N and 12L5417N, respectively. A. J. C. acknowledges Sven Pletincx, Min Tu, Max Lutz Tietze, Aleksander Matavž, Silvia Armini, Sabina Rodríguez-Hermida, Michel De Cooman, Kitty Baert, Johan Meersschaut, Jill Serron, and Nathalie Wauteraerts for scientific support.

References

- I. Stassen, N. Burtch, A. Talin, P. Falcaro, M. Allendorf and R. Ameloot, *Chem. Soc. Rev.*, 2017, **46**, 3185–3241.
- M. D. Allendorf, A. Schwartzberg, V. Stavila and A. A. Talin, *Chem. – Eur. J.*, 2011, **17**, 11372–11388.
- I. Stassen, M. Styles, G. Greci, H. V. Gorp, W. Vanderlinden, S. D. Feyter, P. Falcaro, D. D. Vos, P. Vereecken and R. Ameloot, *Nat. Mater.*, 2016, **15**, 304–310.
- A. J. Cruz, I. Stassen, M. Krishtab, K. Marcoen, T. Stassin, S. Rodríguez-Hermida, J. Teyssandier, S. Pletincx, R. Verbeke, V. Rubio-Giménez, S. Tatay, C. Martí-Gastaldo, J. Meersschaut, P. M. Vereecken, S. De Feyter, T. Hauffman and R. Ameloot, *Chem. Mater.*, 2019, **31**, 9462–9471.
- P. Xu, M. Liu, X. Li, T. Xu and Y. Zhang, in 2017 19th International Conference on Solid-State Sensors, Actuators and Microsystems (TRANSDUCERS), 2017, pp. 762–765.
- P. Rocío-Bautista, A. Gutiérrez-Serpa, A. J. Cruz, R. Ameloot, J. H. Ayala, A. M. Afonso, J. Pasán, S. Rodríguez-Hermida and V. Pino, *Talanta*, 2020, **215**, 120910.
- C. Young, J. Wang, J. Kim, Y. Sugahara, J. Henzie and Y. Yamauchi, *Chem. Mater.*, 2018, **30**, 3379–3386.
- R. Bo, M. Taheri, B. Liu, R. Ricco, H. Chen, H. Amenitsch, Z. Fusco, T. Tsuzuki, G. Yu, R. Ameloot, P. Falcaro and A. Tricoli, *Adv. Sci.*, 2020, **7**, 2002368.
- W. Li, P. Su, Z. Li, Z. Xu, F. Wang, H. Ou, J. Zhang, G. Zhang and E. Zeng, *Nat. Commun.*, 2017, **8**, 406.
- X. Ma, P. Kumar, N. Mittal, A. Khlyustova, P. Daoutidis, K. A. Mkhoyan and M. Tsapatsis, *Science*, 2018, **361**, 1008–1011.
- M. Krishtab, I. Stassen, T. Stassin, A. J. Cruz, O. O. Okudur, S. Armini, C. Wilson, S. De Gendt and R. Ameloot, *Nat. Commun.*, 2019, **10**, 3729.
- T. Stassin, I. Stassen, J. Marreiros, A. J. Cruz, R. Verbeke, M. Tu, H. Reinsch, M. Dickmann, W. Egger, I. F. J. Vankelecom, D. E. De Vos and R. Ameloot, *Chem. Mater.*, 2020, **32**, 1784–1793.
- M. Tu, B. Xia, D. E. Kravchenko, M. L. Tietze, A. J. Cruz, I. Stassen, T. Hauffman, J. Teyssandier, S. De Feyter, Z. Wang, R. A. Fischer, B. Marmiroli, H. Amenitsch, A. Torvisco, M. de J. Velásquez-Hernández, P. Falcaro and R. Ameloot, *Nat. Mater.*, 2021, **20**, 93–99.
- T. Stassin, S. Rodríguez-Hermida, B. Schrode, A. J. Cruz, F. Carraro, D. Kravchenko, V. Creemers, I. Stassen, T. Hauffman, D. D. Vos, P. Falcaro, R. Resel and R. Ameloot, *Chem. Commun.*, 2019, **55**, 10056–10059.
- T. Stassin, I. Stassen, N. Wauteraerts, A. J. Cruz, M. Kräuter, A. M. Coclite, D. De Vos and R. Ameloot, *Eur. J. Inorg. Chem.*, 2020, 71–74.
- D. E. Kravchenko, A. J. Cruz, S. Rodríguez-Hermida, N. Wauteraerts, T. Hauffman and R. Ameloot, *Chem. Mater.*, 2020, **32**, 10469–10475.
- L. He, L. Li, T. Wang, H. Gao, G. Li, X. Wu, Z. Su and C. Wang, *Dalton Trans.*, 2014, **43**, 16981–16985.
- C. Woll, *Prog. Surf. Sci.*, 2007, **82**, 55–120.
- J. Dendooven, K. Devloo-Casier, E. Levrau, R. Van Hove, S. Pulinthanathu Sree, M. R. Baklanov, J. A. Martens and C. Detavernier, *Langmuir*, 2012, **28**, 3852–3859.
- H. Kashima, N. Okamoto and T. Saito, in 2018 20th International Conference on Electronic Materials and Packaging (EMAP), 2018, pp. 1–3.
- J. Holopainen, M. J. Heikkilä, L. D. Salmi, K. Ainassaari and M. Ritala, *Microporous Mesoporous Mater.*, 2018, **267**, 212–220.
- T. Stassin, R. Verbeke, A. J. Cruz, S. Rodríguez-Hermida, I. Stassen, J. Marreiros, M. Krishtab, M. Dickmann, W. Egger, I. F. J. Vankelecom, S. Furukawa, D. D. Vos, D. Grosso, M. Thommes and R. Ameloot, *Adv. Mater.*, 2021, 2006993.
- D. Choudhury, G. Rajaraman and S. K. Sarkar, *RSC Adv.*, 2015, **5**, 29947–29952.
- M. Aghaee, J.-P. Niemelä, W. M. M. Kessels and M. Creatore, *Dalton Trans.*, 2019, **48**, 3496–3505.

- 25 B. Yoon, J. L. O'Patchen, D. Seghete, A. S. Cavanagh and S. M. George, *Chem. Vap. Deposition*, 2009, **15**, 112–121.
- 26 J. Marreiros, L. V. Dommelen, G. Fleury, R. de Oliveira-Silva, T. Stassin, P. Iacomì, S. Furukawa, D. Sakellariou, P. L. Llewellyn, M. Roeffaers and R. Ameloot, *Angew. Chem., Int. Ed.*, 2019, **58**, 18471–18475.
- 27 J. R. Rumble and J. Rumble, *CRC Handbook of Chemistry and Physics*, CRC Press LLC, 98th edn, 2017.
- 28 A. I. Abdulagatov, R. A. Hall, J. L. Sutherland, B. H. Lee, A. S. Cavanagh and S. M. George, *Chem. Mater.*, 2012, **24**, 2854–2863.
- 29 A. Perrotta, R. Berger, F. Muralter and A. M. Coclite, *Dalton Trans.*, 2019, **48**, 14178–14188.